Research Square

Preprints are preliminary reports that have not undergone peer review.
They should not be considered conclusive, used to inform clinical practice,
or referenced by the media as validated information.

High-fat diet-induced MAFLD disrupts sleep architecture through hippocampal neuroinflammation and bifurcated IRS-1/Akt/mTOR signaling in mice

Haitao Zhao
Beijing Friendship Hospital
Peijun Gui
Beijing Friendship Hospital
Bo Zhang
Beijing Friendship Hospital
Jian Wu
Beijing Friendship Hospital
Ying Xie
xieying@ccmu.edu.cn

Beijing Friendship Hospital

Research Article

Keywords: MAFLD, Hippocampus, Sleep architecture, Neuroinflammation

Posted Date: June 29th, 2026

DOI: https://doi.org/10.21203/rs.3.rs-9979296/v1

License: This work is licensed under a Creative Commons Attribution 4.0 International License.
Read Full License

Additional Declarations: No competing interests reported.

Version of Record: A version of this preprint was published at Metabolic Brain Disease on October 26th, 2026. See the published version at https://doi.org/10.1007/s11011-026-02015-3.

Abstract

Background/Aims:

Epidemiological associations between metabolic dysfunction-associated fatty liver disease (MAFLD) and sleep disturbances point to shared mechanisms, yet the underlying central pathways remain unexplored. We hypothesized that high-fat diet (HFD)-induced MAFLD disrupts sleep architecture via hippocampal neuroinflammation and dysregulation of the IRS-1/Akt/mTOR signaling axis.

Methods

Male BALB/c mice were fed a control diet (CD) or a 60% HFD for 16 weeks to induce MAFLD. Sleep–wake architecture was assessed by 24-h EEG/EMG recordings. We evaluated hepatic steatosis, serum cytokines, hippocampal histology, and pro-inflammatory cytokines. Hippocampal expression and phosphorylation of IRS-1 (Ser307), Akt (Ser473), and mTOR (Ser2448) were analyzed by Western blot.

Results

HFD-fed mice developed hepatic steatosis, elevated liver enzymes, and increased serum TNF-α and IL-1β. These mice exhibited reduced non-rapid eye movement (NREM) and rapid eye movement (REM) sleep duration, severe sleep fragmentation (reflected by increased bout numbers and shorter mean bout durations), and diminished NREM sleep delta power. Cosinor analysis revealed a dampened circadian rhythm of NREM sleep delta power. In the hippocampus, HFD induced neuronal injury, elevated TNF-α and IL-1β levels, and a bifurcated signaling profile: increased p-IRS-1 (Ser307), decreased p-Akt (Ser473), yet paradoxically elevated p-mTOR (Ser2448).

Conclusion

Our findings establish a novel liver–hippocampus–sleep axis in which MAFLD-driven systemic inflammation and hippocampal IRS-1/Akt/mTOR dysregulation are associated with profound sleep disruption. Targeting this axis may offer new therapeutic strategies for sleep disorders in MAFLD.

1. Introduction

Metabolic dysfunction-associated fatty liver disease (MAFLD), formerly termed nonalcoholic fatty liver disease (NAFLD), has emerged as the most prevalent chronic liver condition worldwide, driven largely by the global increase in high-fat diet (HFD) consumption and obesity (Eslam, Sanyal, & George, 2020; Younossi et al., 2023). Beyond its well-characterized metabolic and hepatic consequences, MAFLD is now epidemiologically associated with a range of sleep disturbances, including shortened sleep duration, poor sleep quality, and fragmented sleep architecture (Marin-Alejandre et al., 2019; Yang et al.,

2023). Clinically, patients with MAFLD show reduced non-rapid eye movement (NREM) sleep and increased sleep fragmentation, while rodent models of HFD-induced obesity similarly exhibit disrupted slow-wave sleep and altered rapid eye movement (REM) periodicity (Evans et al., 2024; Marin-Alejandre et al., 2019). This bidirectional relationship implies that shared pathophysiological mechanisms may link hepatic steatosis to central sleep regulation; however, the neural substrates and molecular cascades through which a fatty liver communicates with sleep-regulatory circuits remain almost entirely unexplored.

The hippocampus is increasingly recognized not only as a hub for learning and memory but also as a critical node in sleep–wake regulation. Hippocampal sharp-wave ripples and theta oscillations are temporally coupled to NREM and REM sleep, respectively, and the integrity of these sleep-dependent rhythms is exquisitely sensitive to metabolic state (Brodt, Inostroza, Niethard, & Born, 2023; Klinzing, Niethard, & Born, 2019). The hippocampus abundantly expresses insulin receptors and is notably vulnerable to metabolic and inflammatory insults: both systemic insulin resistance and low-grade inflammation impair hippocampal neuronal function, promote pro-inflammatory cytokine release, and disrupt signaling cascades that govern sleep–wake architecture (Kellar & Craft, 2020; Kullmann et al., 2016). Although hippocampal insulin resistance and neuroinflammation have been extensively studied in the context of cognitive decline, their potential role in sleep regulation—another hippocampus-dependent process—has not been examined. This gap is particularly relevant because MAFLD is known to elevate circulating free fatty acids and pro-inflammatory mediators that can compromise blood–brain barrier integrity and directly trigger hippocampal inflammatory responses (Braun & Iliff, 2020; Zhao, Nelson, Betsholtz, & Zlokovic, 2015).

A critical missing link is how hepatic steatosis itself impinges on hippocampal function to alter sleep. Several lines of evidence point to plausible conduits: MAFLD is characterized by elevated circulating free fatty acids, pro-inflammatory cytokines such as tumor necrosis factor-α (TNF-α) and interleukin-6 (IL-6), and dysregulated adipokine profiles (Azzu, Vacca, Virtue, Allison, & Vidal-Puig, 2020; Friedman, Neuschwander-Tetri, Rinella, & Sanyal, 2018). These circulating factors can compromise blood–brain barrier integrity and directly trigger hippocampal inflammatory signaling via toll-like receptors, thereby initiating local neuroinflammation (Xiao et al., 2025; Zlokovic, 2008). The resulting hippocampal pathology may then dysregulate the finely tuned oscillatory networks required for normal sleep architecture, offering a direct mechanistic link from hepatic steatosis to sleep disruption.

Among the pathways that integrate metabolic and inflammatory signals, the insulin receptor substrate-1 (IRS-1)/Akt/mammalian target of rapamycin (mTOR) axis stands out as a central regulator of cellular metabolism, neuronal function, and neuroinflammation. In peripheral tissues, HFD promotes serine phosphorylation of IRS-1, impairing downstream Akt activation and unleashing inflammatory mediators (Armanini, Boscaro, Bordin, & Sabbadin, 2022). A similar process of central insulin resistance has been documented in the hippocampus of obese rodents, where IRS-1/Akt dysregulation contributes to neuronal dysfunction and neuroinflammation (Kothari et al., 2017). Dysregulated mTOR signaling further amplifies neuroinflammation by modulating inflammatory signaling and cytokine synthesis (Li et al.,

2022). Although the IRS-1/Akt/mTOR pathway is well established in both peripheral metabolism and hippocampal neuronal function, whether it mediates the communication between hepatic steatosis and hippocampal-dependent sleep disruption has not been addressed.

In the present study, we tested the hypothesis that HFD-induced MAFLD provokes hippocampal neuroinflammation and insulin resistance through the IRS-1/Akt/mTOR pathway, thereby altering NREM and REM sleep patterns and overall sleep quality. By combining metabolic phenotyping, polysomnographic recordings, and molecular dissection of hippocampal signaling, we sought to uncover a novel liver–hippocampus–sleep axis. To our knowledge, this is the first study to establish a functional connection from diet-induced hepatic steatosis to disrupted sleep architecture via hippocampal insulin resistance and neuroinflammation, addressing a critical gap in our understanding of how metabolic liver disease alters brain function and behavior.

2. Materials and Methods

2.1. Animals and Experimental Design

All animal experiments were approved by the Animal Care and Use Committee of Beijing Friendship Hospital (Ethics Approval No. 2026011314002083). Six-week-old male BALB/c mice (*n* = 6 per group, *N* = 12 total) were obtained from SPF Biotech (Beijing, China). Following one week of acclimatization, mice were randomly assigned to two groups: (1) a control diet (CD) group, fed a standard chow diet (SPF-F02), and (2) a HFD group, fed a diet containing 60% kcal from fat (Research Diets, D12492) to induce hepatic steatosis and metabolic dysfunction. The dietary intervention lasted for 16 weeks. Mice were housed under specific pathogen-free conditions (temperature: 22 ± 1°C; humidity: 55 ± 5%; 12-h light/dark cycle, lights on at 08:00) with *ad libitum* access to food and water. Body weight and food intake were monitored weekly.

2.2. EEG Electrode Implantation and Sleep Recording

At 21 weeks of age (after 15 weeks of dietary intervention), mice were deeply anesthetized with isoflurane (5% for induction, 1.5–2% for maintenance) and surgically implanted with electroencephalography (EEG) and electromyography (EMG) electrodes for polysomnographic recording. Two stainless steel screw electrodes were implanted epidurally over the frontal cortex (coordinates: 1.5 mm lateral, 1.0 mm anterior to bregma) and parietal cortex (1.5 mm lateral, 1.0 mm anterior to lambda). EEG signals were recorded differentially between these two electrodes. For EMG recording, two flexible, Teflon-coated stainless-steel wires were inserted bilaterally into the nuchal trapezius muscle. All electrodes were connected to a miniature 6-pin connector (Pinnacle Technology, USA) and fixed to the skull with dental cement. After surgery, mice were singly housed and allowed 14 days of recovery and acclimation in the recording chambers. Given that long-term electrode implantation (> 16 weeks) carries a high risk of connector detachment and signal degradation in mice, electrodes were implanted near the end of the dietary intervention rather than at baseline. Consequently, sleep recordings were analyzed as

a between-group comparison of the chronic HFD state versus the control state, without a pre-diet baseline.

At 23 weeks of age (after 16 weeks of dietary intervention and 14 days of post-surgical recovery), continuous 24-h video-EEG/EMG signals were recorded in the home cage using the Sirenia Acquisition System (Pinnacle Technology, USA) starting at light offset (20:00). Signals were amplified, filtered (EEG: 0.5–100 Hz; EMG: 10–100 Hz), and digitized at 500 Hz. Sleep–wake states (Wakefulness, NREM sleep, REM sleep) were scored offline manually in 10-s epochs by an experienced investigator blinded to group assignment, according to standard criteria: Wakefulness (low-amplitude, high-frequency EEG with high and variable EMG tone), NREM sleep (high-amplitude, low-frequency EEG dominated by delta activity with low EMG tone), and REM sleep (low-amplitude EEG dominated by regular theta rhythm with muscle atonia). Parameters analyzed included total duration, number of bouts, and mean bout duration for each state across the 12-h dark phase, 12-h light phase, and the entire 24-h period.

NREM sleep EEG power spectral analysis was performed using Fast Fourier Transform (FFT) with a Hanning window on consecutive 5-s epochs within scored NREM sleep. Absolute delta power (1–4 Hz) was calculated for each epoch and averaged across the recording period. The circadian rhythms of NREM sleep delta power and total wake time were analyzed using a cosinor model with a fixed 24-h period, from which mesor, amplitude, and acrophase were derived.

2.3. Sample Collection and Processing

Immediately after the 24-h sleep recording session, mice were fasted for 6 h and then deeply anesthetized with isoflurane. Blood was collected via cardiac puncture, allowed to clot for 30 min at room temperature, and centrifuged at 3,000 × *g* for 15 min at 4°C to obtain serum, which was stored at −80°C. Mice were then transcardially perfused with ice-cold 0.9% saline. The liver and whole brain were rapidly dissected.

For liver tissue, the right lateral lobe was divided into two portions: one portion was snap-frozen in liquid nitrogen and stored at − 80°C for Oil Red O staining of fresh-frozen sections; the other portion was fixed in 4% paraformaldehyde (PFA) in 0.1 M phosphate buffer (pH 7.4) for 48 h at 4°C, then transferred to 70% ethanol and stored at 4°C until paraffin embedding for hematoxylin and eosin (H&E) staining.

For brain tissue, the left hippocampus was rapidly dissected from the left hemisphere on a chilled surface, snap-frozen in liquid nitrogen, and stored at − 80°C for cytokine measurements and Western blot analysis. The right brain hemisphere (containing the right hippocampus) was fixed in 4% PFA for 48 h at 4°C, then transferred to 70% ethanol and stored at 4°C until paraffin embedding for Nissl staining.

2.4. Serum Biochemical Assays

Serum levels of alanine aminotransferase (ALT), aspartate aminotransferase (AST), total cholesterol (TC), and triglycerides (TG) were measured using commercial enzymatic colorimetric assay kits (Acmec, China; Cat# AC10334, AC10336, AC10369, and AC10178, respectively) according to the manufacturer's

instructions. Serum concentrations of the pro-inflammatory cytokines TNF-α and interleukin-1 beta (IL-1β) were quantified using specific enzyme-linked immunosorbent assay (ELISA) kits (Acmec, China; Cat# AC16568 and AC16536, respectively) following the manufacturer's protocols.

2.5. Histological Analysis

2.5.1. Liver Histology

For H&E staining, fixed liver tissues were dehydrated, embedded in paraffin, and sectioned at 4 μm thickness. For Oil Red O (ORO) staining, the snap-frozen liver tissue was embedded in OCT compound (Solarbio, China), sectioned at 8 μm thickness using a cryostat, and stained with an ORO staining kit (Solarbio, China) according to the manufacturer's protocol. All sections were imaged using a Zeiss Axio Observer A1 light microscope (Zeiss, Germany).

2.5.2. Hippocampal Histology

The fixed right brain hemisphere was dehydrated, embedded in paraffin, and coronally sectioned at 4 μm thickness. Sections encompassing the dorsal hippocampus were dewaxed, rehydrated, and stained with Cresyl Violet (Nissl) staining solution (Solarbio, China) for 15 min. After differentiation and dehydration, sections were mounted with neutral balsam for observation. The morphology of pyramidal neurons in the hippocampal CA1 region was examined and imaged under a light microscope (Zeiss Axio Observer A1, Zeiss, Germany).

2.6. Hippocampal Cytokine Measurements

Frozen left hippocampal tissue was weighed, homogenized in ice-cold PBS containing protease inhibitors, and centrifuged at 12,000 × *g* for 20 min at 4°C. The supernatant was collected, and total protein concentration was determined by BCA assay. Levels of TNF-α and IL-1β in hippocampal homogenates were measured using the same ELISA kits as for serum (Acmec, China; Cat# AC16568 and AC16536).

2.7. Western Blot Analysis

Frozen left hippocampal tissues were homogenized in RIPA lysis buffer (Beyotime, China) supplemented with 1% protease and phosphatase inhibitor cocktails (Thermo Fisher Scientific, USA). Protein concentration was determined using a BCA protein assay kit (Beyotime, China). Equal amounts of protein (30 μg) were separated by 10% SDS-PAGE and transferred to PVDF membranes (Millipore, USA). Membranes were blocked with 5% non-fat milk in TBST for 1 h at room temperature and then incubated overnight at 4°C with the following primary antibodies: rabbit monoclonal anti-phospho-IRS-1 (Ser307) (1:1000; Abcam, Cat# ab5599), rabbit polyclonal anti-IRS-1 (1:1000; Abcam, Cat# ab245314), rabbit monoclonal anti-phospho-Akt (Ser473) (1:2000; Abcam, Cat# ab81283), rabbit monoclonal anti-Akt (1:1000; Abcam, Cat# ab188099), rabbit monoclonal anti-phospho-mTOR (Ser2448) (1:1000; Abcam, Cat# ab109268), rabbit monoclonal anti-mTOR (1:1000; Abcam, Cat# ab134903), and mouse monoclonal anti-α-tubulin (1:10,000; Abcam, Cat# ab52866). After washing with TBST, membranes were

incubated with corresponding HRP-conjugated secondary antibodies (1:5000) for 1 h at room temperature. Protein bands were visualized using an enhanced chemiluminescence (ECL) substrate (Millipore, USA) and quantified with ImageJ software (NIH, USA). Phosphorylation levels of IRS-1, Akt, and mTOR were normalized to their respective total protein levels. Total protein levels were normalized to α-tubulin.

2.8. Statistical Analysis

All statistical analyses were performed using GraphPad Prism 9.5.1 (GraphPad Software, San Diego, CA, USA). The Shapiro-Wilk test was used to assess normality of data distribution. For two-group comparisons, an unpaired two-tailed Student's *t* -test was applied for normally distributed data, and the Mann-Whitney *U* test was used for non-normally distributed data. NREM delta power across the 24-hour period was analyzed using a 2 (Diet: CD vs. HFD) × 24 (Time) mixed-model ANOVA, with Diet as a between-subjects factor and Time as a within-subjects factor. The circadian rhythm of delta power was analyzed using the Cosinor method. A p - value < 0.05 was considered statistically significant. The experimenter was blinded to group assignments during all data acquisition and analysis stages.

3. Results

3.1. High-fat diet induces hepatic steatosis and systemic metabolic inflammation in mice

Male BALB/c mice were fed either a CD or a HFD for 16 weeks. The experimental timeline (Fig. 1) included a 1-week acclimatization, 16-week dietary intervention, and subsequent sleep recording and tissue collection protocols.

Chronic HFD feeding successfully induced the hallmarks of metabolic syndrome, with pronounced hepatic pathology. Histopathological analysis revealed extensive hepatic steatosis in HFD-fed mice. Representative images of liver sections showed massive intracellular lipid droplet accumulation via Oil Red O (ORO) staining (Fig. 2A, left panels) and severe macrovesicular steatosis via Hematoxylin and Eosin (H&E) staining (Fig. 2A, right panels), consistent with MAFLD.

Biochemical quantification confirmed the histological observations. HFD-fed mice exhibited significantly elevated hepatic lipid content, with TG levels increased to 51.92 ± 2.91 mg/g tissue (vs. CD: 24.14 ± 2.57 mg/g tissue, t (9.85) = 17.52, p < 0.0001) and TC levels increased to 5.33 ± 0.30 mg/g tissue (vs. CD: 2.35 ± 0.32 mg/g tissue, t (9.94) = 16.59, p < 0.0001) (Fig. 2B, C). This was accompanied by significant liver injury, as indicated by elevated serum levels of ALT (CD: 57.25 ± 7.10 U/L, HFD: 99.81 ± 7.29 U/L, t (9.99) = 10.24, p < 0.0001) and AST (CD: 75.79 ± 10.02 U/L, HFD: 142.00 ± 15.48 U/L, t (8.57) = 8.80·, p < 0.0001) (Fig. 2D, E).

Furthermore, HFD induced a state of systemic low-grade inflammation, a key feature linking peripheral metabolism to central nervous system dysfunction. Serum levels of the pro-inflammatory cytokines TNF-

α and IL-1β were markedly higher in the HFD group (TNF-α: CD: 1.73 ± 0.15 pg/μL, HFD: 2.29 ± 0.31 pg/μL, t (7.18) = 3.96, $p < 0.01$; IL-1β: CD: 0.26 ± 0.02 pg/μL, HFD: 0.36 ± 0.02 pg/μL, t (9.41) = 7.68, $p < 0.0001$) (Fig. 2F, G).

Together, these data demonstrate that 16 weeks of HFD feeding robustly induces hepatic steatosis, liver damage, and a systemic pro-inflammatory state, establishing a valid model of diet-induced metabolic dysfunction for investigating its downstream effects on brain function and sleep architecture.

3.2 HFD disrupts sleep architecture, induces severe fragmentation, and impairs circadian rhythmicity

To determine the effects of HFD on sleep homeostasis and circadian regulation, we performed continuous 24-h EEG/EMG recordings in HFD-fed and CD-fed mice (Fig. 3A, B). Given that hippocampal sharp-wave ripples and slow-wave activity is predominantly expressed during NREM sleep and are critically involved in sleep-dependent synaptic homeostasis, we focused our spectral power and circadian rhythm analyses on NREM sleep. REM sleep was assessed for total duration and fragmentation to provide a complete sleep architectural profile.

3.2.1 HFD reduces total sleep duration and alters sleep–wake macrostructure

Analysis of total sleep duration revealed marked changes in sleep macrostructure (Fig. 3C, F, I). Compared to CD mice, HFD mice exhibited a pronounced reduction in total 24-h NREM sleep (Fig. 3C; CD: 564.90 ± 18.13 min; HFD: 451.60 ± 10.62 min, t (8.07) = 13.21, $p < 0.0001$). This reduction was primarily attributable to a substantial decrease during the light (rest) phase, whereas the dark phase showed a smaller but consistent trend, see Table 1 for detailed data.

Table 1
Sleep–wake parameters in CD and HFD mice.

NREM sleep		**Phase**	**CD**	**HFD**	**Test statistic**	***P* value**
	Time(min)	**dark**	**244.10 ± 12.07**	**271.90 ± 11.37**	***t* = 4.10**	**0.002**
		light	320.90 ± 16.99	179.70 ± 10.16	*t* = 17.46	< 0.0001
		24hour	564.90 ± 18.13	451.60 ± 10.62	*t* = 13.21	< 0.0001
	Bouts(n)	dark	90.33 ± 11.79	152.80 ± 12.17	*t* = 9.03	< 0.0001
		light	90.33 ± 6.77	174.30 ± 9.97	*t* = 17.07	< 0.0001
		24hour	180.70 ± 8.29	327.20 ± 15.52	*t* = 20.39	< 0.0001
	Duration(min)	dark	2.73 ± 0.26	1.79 ± 0.14	*t* = 7.85	< 0.0001
		light	3.56 ± 0.25	1.03 ± 0.08	*t* = 23.41	< 0.0001
		24hour	3.13 ± 0.18	1.38 ± 0.06	*t* = 23.07	< 0.0001
REM sleep	Time(min)	dark	46.27 ± 7.54	36.13 ± 14.25	*t* = 1.54	0.1642
		light	60.37 ± 11.57	24.98 ± 6.47	*t* = 6.54	0.0002
		24hour	106.60 ± 14.48	61.12 ± 16.35	*t* = 5.11	0.0005
	Bouts(n)	dark	30.67 ± 5.75	39.00 ± 13.71	*t* = 1.37	0.21
		light	27.50 ± 3.94	35.83 ± 7.18	*t* = 2.50	0.038
		24hour	58.17 ± 4.75	74.83 ± 10.57	*t* = 3.52	0.0098
	Duration(min)	dark	1.39[1.20,2.26]	0.66[0.51,2.26]	*U* = 10	0.2165
		light	2.19 ± 0.24	0.70 ± 0.15	*t* = 12.92	< 0.0001
		24hour	1.80[1.61,2.15]	0.66[0.57,1.37]	*U = 0*	0.0022
WAKE	Time(min)	dark	428.80 ± 16.78	413.60 ± 9.94	*t* = 1.91	0.0918
		light	336.00 ± 16.20	512.00 ± 17.01	*t* = 18.35	< 0.0001

NREM sleep		Phase	CD	HFD	Test statistic	*P* value
	Time(min)	**dark**	**244.10 ± 12.07**	**271.90 ± 11.37**	***t* = 4.10**	**0.002**
		24hour	764.80 ± 9.54	925.60 ± 19.14	*t* = 18.41	< 0.0001
	Bouts(n)	dark	75.50 ± 4.37	56.50 ± 3.67	*t* = 8.15	< 0.0001
		light	68.33 ± 6.83	87.83 ± 4.31	*t* = 5.91	0.0003
		24hour	143.80 ± 4.88	144.30 ± 6.35	*t* = 0.15	0.8816
	Duration(min)	dark	5.70 ± 0.52	7.34 ± 0.48	*t* = 5.72	0.0002
		light	4.97 ± 0.66	5.85 ± 0.42	*t* = 2.75	0.0235
		24hour	5.32 ± 0.18	6.42 ± 0.30	*t* = 7.76	< 0.0001

Data are presented as mean ± SD for normally distributed variables and median [interquartile range] for non-normally distributed variables (REM duration, Dark and 24 h). Normally distributed data were compared using unpaired two-tailed Student's *t*-test; non-normally distributed data were compared using Mann-Whitney *U* test. *n* = 6 per group. CD, control diet; HFD, high-fat diet; NREM, non-rapid eye movement; REM, rapid eye movement.

Similarly, REM sleep was severely compromised in HFD-fed mice (Fig. 3F). Total 24-h REM sleep duration was significantly reduced (CD: 106.60 ± 14.48 min; HFD: 61.12 ± 16.35 min, t (9.86) = 5.10, $p < 0.001$), again largely reflecting deficits in the light phase. In contrast, total wakefulness was significantly increased in HFD mice (Fig. 3I; CD: 764.80 ± 9.54 min; HFD: 925.60 ± 19.14 min, t (7.34) = 18.41, $p < 0.0001$ for 24 h), indicating that HFD mice fail to sustain sleep during their natural rest period.

3.2.2 HFD induces severe sleep fragmentation

Beyond total sleep duration, HFD profoundly disrupted sleep continuity. For NREM sleep, HFD mice displayed a striking increase in the number of bouts (Fig. 3D) accompanied by a marked reduction in mean NREM sleep bout duration (Fig. 3E). Mean NREM sleep bout length was significantly shorter in HFD mice over 24 h (CD: 3.13 ± 0.18 min; HFD: 1.38 ± 0.06 min, t (6.11) = 23.07, $p < 0.0001$), a pattern that persisted across both dark and light phases.

Sleep fragmentation was even more pronounced for REM sleep. HFD mice exhibited significantly more REM bouts (Fig. 3G) and a drastically shorter mean REM bout duration (Fig. 3H; CD: median = 1.79 min; HFD: median = 0.66 min, Mann-Whitney U = 0, $p < 0.01$ for 24 h), indicating that HFD mice are incapable of sustaining REM sleep episodes.

Interestingly, while the number of wake bouts was only moderately altered (Fig. 3J), the mean wake bout duration was significantly increased in HFD mice (Fig. 3K; CD: 5.32 ± 0.18 min; HFD: 6.42 ± 0.30 min, t (8.09) = 7.76, $p < 0.0001$ for 24 h), suggesting that once awakened, HFD mice remain awake longer, further aggravating sleep loss.

3.2.3 HFD attenuates slow-wave activity during NREM sleep

EEG spectral analysis during NREM sleep (Fig. 3L) revealed that HFD significantly suppressed power in the low-frequency delta band (1–4 Hz), a hallmark of restorative slow-wave sleep. A two-way repeated-measures ANOVA with frequency as the within-subject factor and diet as the between-subject factor showed a significant main effect of diet (Column Factor: F (1, 10) = 21.11, $p = 0.001$), indicating that overall delta power was lower in HFD-fed mice. Post-hoc comparisons confirmed that HFD mice exhibited significantly reduced power at each integer frequency from 1 to 4 Hz (1 Hz: CD: 99.15 ± 39.16 μV², HFD: 41.52 ± 12.03 μV², t (5.93) = 3.45, $p < 0.05$; 2 Hz: CD: 123.50 ± 46.76 μV², HFD: 37.84 ± 6.62 μV², t (5.20) = 4.45, $p < 0.01$; 3 Hz: CD: 109.70 ± 38.93 μV², HFD: 29.06 ± 2.95 μV², t (5.06) = 5.06, $p < 0.01$; 4 Hz: CD: 83.43 ± 27.41 μV², HFD: 20.67 ± 1.83 μV², t (5.04) = 5.60, $p < 0.01$). The mean delta power averaged across the 1–4 Hz band was markedly reduced in HFD mice.

3.2.4 HFD blunts the circadian amplitude of NREM sleep

Cosinor rhythmometry of NREM sleep delta power over the 24-h cycle (Fig. 3M, N) revealed a dampened circadian rhythm in HFD mice. All three cosinor parameters were significantly altered compared with CD controls. The 24-h adjusted mean (mesor) was markedly lower (CD: 102.50 ± 6.06; HFD: 54.24 ± 7.32, t (9.66) = 12.44, $p < 0.0001$). Rhythm amplitude was severely blunted (CD: 50.80 ± 4.77; HFD: 15.43 ± 8.05, t (8.13) = 9.26, $p < 0.0001$), and a significant phase advance was observed (CD: 12.03 ± 1.90; HFD: 8.29 ± 1.96, t (9.99) = 3.35, $p < 0.01$). These findings demonstrate that HFD not only reduces sleep quantity and fragments sleep but also impairs the robustness of the circadian clock governing sleep–wake patterns, as reflected by a reduced mesor, diminished amplitude, and shifted phase.

3.3 HFD induces hippocampal neuroinflammation and dysregulates insulin/insulin-like signaling pathways

To investigate the underlying mechanisms of HFD-induced hippocampal injury, we examined histological morphology, neuroinflammatory cytokine levels, and the expression/phosphorylation of key insulin signaling pathway proteins.

Nissl staining revealed distinct morphological changes in the hippocampal CA region (Fig. 4A). In CD mice, hippocampal neurons were densely packed and structurally intact. In contrast, the HFD group exhibited noticeable neuronal disorganization, cytoplasmic shrinkage, and looser tissue architecture. We then measured hippocampal pro-inflammatory cytokine levels. HFD significantly increased TNF-α (CD: 148.30 ± 2.73 pg/mg; HFD: 200.00 ± 24.33 pg/mg, t (5.13) = 5.17, $p < 0.01$) and IL-1β (CD: 18.33 ± 2.49 pg/mg; HFD: 28.42 ± 4.34 pg/mg, t (7.97) = 4.94, $p < 0.01$) (Fig. 4B, C).

To explore the molecular underpinnings, we analyzed key nodes of the insulin signaling pathway by Western blot. Total IRS-1 protein levels were reduced in the HFD group compared with CD controls (Fig. 4E). HFD significantly increased IRS-1 phosphorylation at Ser307 (Fig. 4D, F), resulting in an elevated p-IRS-1 (Ser307)/IRS-1 ratio (CD: 0.84 ± 0.10; HFD: 1.21 ± 0.08, t (3.81) = 5.27, $p < 0.01$).

Analysis of the downstream effector Akt revealed suppressed activity (Fig. 4G–I). Total Akt levels did not differ between groups (Fig. 4H, NS), but Akt phosphorylation at Ser473 was markedly reduced in HFD mice. Accordingly, the p-Akt (Ser473)/Akt ratio was significantly lower in HFD-fed mice (Fig. 4I; CD: 0.97 ± 0.02; HFD: 0.29 ± 0.04, t (2.87) = 26.95, $p < 0.001$).

Finally, we examined mTOR phosphorylation status (Fig. 4J–L). Interestingly, despite the reduction in p-Akt (Ser473), HFD significantly increased mTOR phosphorylation at Ser2448 (Fig. 4J). Total mTOR levels were comparable between groups (Fig. 4K, NS). Quantification confirmed a robust increase in the p-mTOR (Ser2448)/mTOR ratio in HFD mice (Fig. 4L; CD: 0.79 ± 0.19; HFD: 1.44 ± 0.03, t (2.10) = 5.80, $p < 0.05$).

Collectively, these results demonstrate that HFD induces marked structural damage and neuroinflammation in the hippocampus, accompanied by aberrant insulin signaling characterized by increased p-IRS-1 (Ser307), decreased p-Akt (Ser473), and paradoxical hyperactivation of mTOR signaling via elevated p-mTOR (Ser2448).

4. Discussion

In the present study, we demonstrate that chronic HFD-induced MAFLD triggers pronounced sleep disruption, accompanied by hippocampal neuroinflammation and dysregulation of the IRS-1/Akt/mTOR signaling axis. To our knowledge, this is the first study to establish a functional link from diet-induced hepatic steatosis to disrupted sleep via hippocampal insulin resistance and neuroinflammation, providing a mechanistic framework for the well-documented epidemiological association between metabolic liver disease and sleep disturbances.

Consistent with prior reports, 16 weeks of HFD feeding induced hallmark features of MAFLD, including hepatic steatosis, elevated liver enzymes, and a systemic pro-inflammatory state (Friedman et al., 2018; Younossi et al., 2023). The sleep phenotype we observed—reduced NREM and REM sleep, severe fragmentation, and diminished NREM sleep delta power—closely mirrors sleep disturbances reported in MAFLD patients (Wang et al., 2025) and in rodent models of diet-induced obesity (Evans et al., 2024). Importantly, these sleep abnormalities were accompanied by clear structural and molecular evidence of hippocampal injury: Nissl staining revealed neuronal disorganization and cytoplasmic shrinkage in CA1, and hippocampal levels of TNF-α and IL-1β were significantly elevated. These findings indicate that the hippocampus, a brain region critically involved in sleep–wake regulation (Feld & Born, 2020; Lutz, Harkotte, & Born, 2026), is a target of MAFLD-driven pathology. The loss of restorative slow-wave activity, reflected by suppressed delta power, further suggests impaired synaptic homeostasis and may account for the non-restorative sleep complaint commonly reported in MAFLD patients (Cirelli & Tononi, 2022).

A key finding is the elevation of pro-inflammatory cytokines in the hippocampus following HFD consumption. Although acutely elevated TNF-α and IL-1β are somnogenic, their chronic, unregulated overproduction can disrupt normal sleep architecture by altering the excitability of sleep-regulatory neurons and weakening the homeostatic sleep drive (Besedovsky, Lange, & Haack, 2019; Irwin & Opp, 2017). In particular, persistently high brain levels of IL-1β have been shown to fragment NREM sleep and suppress slow-wave activity (Krueger, Frank, Wisor, & Roy, 2016). Our observation of elevated hippocampal IL-1β and TNF-α, together with fragmented sleep and reduced delta power, is consistent with this mechanism. The source of these hippocampal cytokines is likely multifactorial: circulating inflammatory mediators, which were elevated in HFD-fed mice, can compromise blood–brain barrier integrity and enter the hippocampal parenchyma, where they stimulate local cytokine production (Brown et al., 2022; Manabe et al., 2021). Although we did not directly assess glial activation, the observed neuronal morphological changes and cytokine elevations strongly suggest an ongoing neuroinflammatory process potentially driven by infiltrating peripheral signals. The present study focused spectral power and circadian rhythm analyses on NREM sleep, a decision grounded in the unique neurophysiological relationship between the hippocampus and NREM sleep. Hippocampal sharp-wave ripples (SPW-Rs), among the most prominent population events in the mammalian brain, occur almost exclusively during NREM sleep and are critically involved in systems memory consolidation and synaptic downscaling(Brodt et al., 2023; Klinzing et al., 2019). The generation and coupling of SPW-Rs with neocortical slow-wave activity is highly sensitive to metabolic and inflammatory states, and insulin signaling has been shown to modulate hippocampal network oscillations underlying NREM sleep(Kellar & Craft, 2020; Kothari et al., 2017; Kullmann et al., 2016). Importantly, the IRS-1/Akt/mTOR axis is a well-established regulator of activity-dependent synaptic plasticity and protein synthesis that contribute to the maintenance of NREM slow-wave activity (Bockaert & Marin, 2015; Seibt & Frank, 2019). Although the hippocampus also generates theta oscillations during REM sleep, the neuroinflammatory and insulin signaling dysfunction observed here is predicted to preferentially impair NREM-dependent processes, providing a mechanistic rationale for our analytical emphasis on NREM sleep.

A central mechanistic finding is the bifurcated pattern of insulin/insulin-like signaling in the hippocampus. Consistent with central insulin resistance, HFD increased inhibitory IRS-1 serine phosphorylation at Ser307 and reduced Akt phosphorylation at Ser473 (Chen, Cai, Hoover, & Kahn, 2022; Zhang, Tian, Hu, & Meng, 2022). Unexpectedly, mTOR phosphorylation at Ser2448 was significantly elevated despite the concomitant suppression of Akt, a canonical upstream activator of mTORC1. This paradox may be explained by Akt-independent inputs to mTORC1 that are enhanced under HFD conditions, such as amino acid signaling via Rag GTPases, direct activation by pro-inflammatory cytokines, or crosstalk with other nutrient-sensing pathways (Gao et al., 2025; Liu & Sabatini, 2020). The resulting mTOR hyperactivity may contribute to sleep disruption by altering protein synthesis-dependent synaptic plasticity processes that underlie slow-wave activity and sleep consolidation (Bockaert & Marin, 2015; Seibt & Frank, 2019). Moreover, mTOR overactivation can feed back to sustain a pro-inflammatory state, potentially creating a vicious cycle that perpetuates hippocampal pathology and sleep

fragmentation. The functional significance of this divergent Akt/mTOR regulation warrants further investigation using pharmacological or genetic approaches to dissect the specific contribution of each branch to sleep phenotypes.

Cosinor analysis revealed a marked dampening of circadian rhythmicity in sleep–wake patterns, evidenced by reduced mesor and amplitude of NREM sleep delta power rhythms. This is consistent with evidence that both MAFLD and central insulin resistance can weaken circadian output (Engin, 2024; Patke, Young, & Axelrod, 2020). Although the hippocampus contributes to consolidating circadian patterns of activity, we cannot exclude contributions from the hypothalamic suprachiasmatic nucleus or peripheral clocks in the liver. Nonetheless, the robust association between hippocampal pathology and circadian dampening supports the view that the proposed liver–hippocampus–sleep axis extends beyond acute sleep architecture to encompass circadian organization.

Several limitations warrant consideration. First, the sample size was modest and only male mice were used, limiting generalizability. Second, the study design is correlative; establishing a causal role for hippocampal IRS-1/Akt/mTOR dysregulation in sleep disruption will require region-specific genetic or pharmacological manipulations. Third, neuroinflammation was assessed solely by cytokine measurements and Nissl staining; detailed characterization of glial phenotypes was not performed and represents an important direction for future studies. Fourth, while mTOR hyperphosphorylation was observed, the precise upstream activator in this context remains to be identified. Furthermore, an important limitation of this study stems from the technical challenges associated with long-term electrode implantation. Due to these constraints, we were unable to record baseline sleep prior to the dietary intervention, thereby precluding a within-subject, pre-post comparison. This limitation makes it impossible to fully exclude potential baseline differences between experimental groups. For future investigations, the use of detachable miniature wireless recording devices could enable such longitudinal assessments.

In summary, this study provides the first integrated evidence that HFD-induced MAFLD is associated with hippocampal neuroinflammation and bifurcated insulin/mTOR signaling, accompanied by profound sleep fragmentation, reduced slow-wave activity, and weakened circadian rhythmicity. These findings delineate a novel liver–hippocampus–sleep axis and identify the IRS-1/Akt/mTOR pathway as a critical signaling node linking metabolic liver disease to central sleep dysregulation. Targeting this axis may offer new therapeutic strategies for sleep disturbances in patients with MAFLD.

Conclusion

In summary, this study demonstrates that chronic high-fat diet-induced MAFLD is associated with profound disruptions of sleep architecture, including reduced NREM and REM sleep, severe sleep fragmentation, diminished NREM slow-wave activity, and weakened circadian rhythmicity. These sleep abnormalities are accompanied by hippocampal neuroinflammation and a bifurcated dysregulation of the IRS-1/Akt/mTOR signaling pathway, characterized by increased inhibitory p-IRS-1 (Ser307),

suppressed p-Akt (Ser473), and paradoxically elevated p-mTOR (Ser2448). Our findings delineate a novel liver–hippocampus–sleep axis and identify hippocampal insulin resistance and mTOR hyperactivation as potential mechanistic links between metabolic liver disease and central sleep dysregulation. Targeting this axis may offer new therapeutic strategies for sleep disorders in patients with MAFLD.

Declarations

Data availability

All data used in this study are available from the corresponding author upon reasonable request.

Funding

This study was supported by the Seed Program of Beijing Friendship Hospital (Grant No. YYZZ202344), Capital's Funds for Health Improvement and Research (Program No. SF2024-2-2027), and the Youth Elite Program of Beijing Freindship Hospital (Program No. YYQCJH2002-10).

Competing interests

The authors declare no competing interests.

Author Contributions

All authors contributed to the study conception and design. Material preparation, data collection and analysis were performed by Haitao Zhao and Peijun Gui. The first draft of the manuscript was written by Haitao Zhao and all authors commented on previous versions of the manuscript. All authors read and approved the final manuscript.

Ethical approval

All animal experiments were conducted in accordance with the guidelines approved by the Beijing Friendship Hospital, Capital Medical University.

References

1. Armanini D, Boscaro M, Bordin L, Sabbadin C (2022) Controversies in the Pathogenesis, Diagnosis and Treatment of PCOS: Focus on Insulin Resistance, Inflammation, and Hyperandrogenism. Int J Mol Sci 23(8):4110. https://doi.org/10.3390/ijms23084110
2. Azzu V, Vacca M, Virtue S, Allison M, Vidal-Puig A (2020) Adipose Tissue-Liver Cross Talk in the Control of Whole-Body Metabolism: Implications in Nonalcoholic Fatty Liver Disease. Gastroenterology 158(7):1899–1912. https://doi.org/10.1053/j.gastro.2019.12.054
3. Besedovsky L, Lange T, Haack M (2019) The Sleep-Immune Crosstalk in Health and Disease. Physiol Rev 99(3):1325–1380. https://doi.org/10.1152/physrev.00010.2018

4. Bockaert J, Marin P (2015) mTOR in Brain Physiology and Pathologies. Physiol Rev 95(4):1157–1187. https://doi.org/10.1152/physrev.00038.2014
5. Braun M, Iliff JJ (2020) The impact of neurovascular, blood-brain barrier, and glymphatic dysfunction in neurodegenerative and metabolic diseases. Int Rev Neurobiol 154:413–436. https://doi.org/10.1016/bs.irn.2020.02.006
6. Brodt S, Inostroza M, Niethard N, Born J (2023) Sleep-A brain-state serving systems memory consolidation. Neuron 111(7):1050–1075. https://doi.org/10.1016/j.neuron.2023.03.005
7. Brown C, Pemberton S, Babin A, Abdulhameed N, Noonan C, Brown MB, Banks WA, Rhea EM (2022) Insulin blood-brain barrier transport and interactions are greater following exercise in mice. Journal of applied physiology (Bethesda, Md.: 1985), 132(3), 824–834. https://doi.org/10.1152/japplphysiol.00866.2021
8. Chen W, Cai W, Hoover B, Kahn CR (2022) Insulin action in the brain: cell types, circuits, and diseases. Trends Neurosci 45(5):384–400. https://doi.org/10.1016/j.tins.2022.03.001
9. Cirelli C, Tononi G (2022) The why and how of sleep-dependent synaptic down-selection. Semin Cell Dev Biol 125:91–100. https://doi.org/10.1016/j.semcdb.2021.02.007
10. Engin A (2024) Misalignment of Circadian Rhythms in Diet-Induced Obesity. Adv Exp Med Biol 1460:27–71. https://doi.org/10.1007/978-3-031-63657-8_2
11. Eslam M, Sanyal AJ, George J, International Consensus Panel (2020) MAFLD: A Consensus-Driven Proposed Nomenclature for Metabolic Associated Fatty Liver Disease. Gastroenterology 158(7):1999–2014. https://doi.org/10.1053/j.gastro.2019.11.312. e1
12. Evans AK, Saw NL, Woods CE, Vidano LM, Blumenfeld SE, Lam RK, Chu EK, Reading C, Shamloo M (2024) Impact of high-fat diet on cognitive behavior and central and systemic inflammation with aging and sex differences in mice. Brain, behavior, and immunity. 118:334–354. https://doi.org/10.1016/j.bbi.2024.02.025
13. Feld GB, Born J (2020) Neurochemical mechanisms for memory processing during sleep: basic findings in humans and neuropsychiatric implications. Neuropsychopharmacology: official publication Am Coll Neuropsychopharmacol 45(1):31–44. https://doi.org/10.1038/s41386-019-0490-9
14. Friedman SL, Neuschwander-Tetri BA, Rinella M, Sanyal AJ (2018) Mechanisms of NAFLD development and therapeutic strategies. Nat Med 24(7):908–922. https://doi.org/10.1038/s41591-018-0104-9
15. Gao R, Xiong Z, Su W, Deng J, Zhai B, Zhu G, Zhang M, Zeng Q, Qiu J, Bian Z, Xiao H, Luan G, Wang R (2025) Microglial Feimin Alleviates Cognitive Impairment in High-Fat Diet-Fed Mice. Advanced science (Weinheim, Baden-Wurttemberg, Germany), 12(48), e12023. https://doi.org/10.1002/advs.202512023
16. Irwin MR, Opp MR (2017) Sleep Health: Reciprocal Regulation of Sleep and Innate Immunity. Neuropsychopharmacology: official publication Am Coll Neuropsychopharmacol 42(1):129–155. https://doi.org/10.1038/npp.2016.148

17. Kellar D, Craft S (2020) Brain insulin resistance in Alzheimer's disease and related disorders: mechanisms and therapeutic approaches. Lancet Neurol 19(9):758–766. https://doi.org/10.1016/S1474-4422(20)30231-3
18. Klinzing JG, Niethard N, Born J (2019) Mechanisms of systems memory consolidation during sleep. Nat Neurosci 22(10):1598–1610. https://doi.org/10.1038/s41593-019-0467-3
19. Kothari V, Luo Y, Tornabene T, O'Neill AM, Greene MW, Geetha T, Babu JR (2017) High fat diet induces brain insulin resistance and cognitive impairment in mice. Biochimica et biophysica acta. Mol basis disease 1863(2):499–508. https://doi.org/10.1016/j.bbadis.2016.10.006
20. Krueger JM, Frank MG, Wisor JP, Roy S (2016) Sleep function: Toward elucidating an enigma. Sleep Med Rev 28:46–54. https://doi.org/10.1016/j.smrv.2015.08.005
21. Kullmann S, Heni M, Hallschmid M, Fritsche A, Preissl H, Häring HU (2016) Brain Insulin Resistance at the Crossroads of Metabolic and Cognitive Disorders in Humans. Physiol Rev 96(4):1169–1209. https://doi.org/10.1152/physrev.00032.2015
22. Li Y, Cheng Y, Zhou Y, Du H, Zhang C, Zhao Z, Chen Y, Zhou Z, Mei J, Wu W, Chen M (2022) High fat diet-induced obesity leads to depressive and anxiety-like behaviors in mice via AMPK/mTOR-mediated autophagy. Exp Neurol 348:113949. https://doi.org/10.1016/j.expneurol.2021.113949
23. Liu GY, Sabatini DM (2020) mTOR at the nexus of nutrition, growth, ageing and disease. Nat Rev Mol Cell Biol 21(4):183–203. https://doi.org/10.1038/s41580-019-0199-y
24. Lutz ND, Harkotte M, Born J (2026) Sleep's contribution to memory formation. Physiol Rev 106(1):363–483. https://doi.org/10.1152/physrev.00054.2024
25. Manabe T, Rácz I, Schwartz S, Oberle L, Santarelli F, Emmrich JV, Neher JJ, Heneka MT (2021) Systemic inflammation induced the delayed reduction of excitatory synapses in the CA3 during ageing. J Neurochem 159(3):525–542. https://doi.org/10.1111/jnc.15491
26. Marin-Alejandre BA, Abete I, Cantero I, Riezu-Boj JI, Milagro FI, Monreal JI, Elorz M, Herrero JI, Benito-Boillos A, Quiroga J, Martinez-Echeverria A, Uriz-Otano JI, Huarte-Muniesa MP, Tur JA, Martínez JA, Zulet MA (2019) Association between Sleep Disturbances and Liver Status in Obese Subjects with Nonalcoholic Fatty Liver Disease: A Comparison with Healthy Controls. Nutrients 11(2):322. https://doi.org/10.3390/nu11020322
27. Patke A, Young MW, Axelrod S (2020) Molecular mechanisms and physiological importance of circadian rhythms. Nat Rev Mol Cell Biol 21(2):67–84. https://doi.org/10.1038/s41580-019-0179-2
28. Seibt J, Frank MG (2019) Primed to Sleep: The Dynamics of Synaptic Plasticity Across Brain States. Front Syst Neurosci 13:2. https://doi.org/10.3389/fnsys.2019.00002
29. Wang Q, Chen H, Deng H, Zhang M, Hu H, Ouyang H, Ma L, Liu R, Sun J, Hu G, Wang K (2025) Association of daily sleep duration with risk of metabolic dysfunction-associated steatotic liver disease and adverse liver outcomes. Diabetes Metab 51(3):101628. https://doi.org/10.1016/j.diabet.2025.101628
30. Xiao W, Yang Y, Bai L, Yang P, Li R, Yang D, Li F, Quan L, Liang Q, Yan Y, Qi T, Liang F (2025) Exercise-induced irisin ameliorates cognitive impairment following chronic cerebral hypoperfusion by

suppressing neuroinflammation and hippocampal neuronal apoptosis. J Neuroinflamm 22(1):168. https://doi.org/10.1186/s12974-025-03493-5

31. Yang J, Zhang K, Xi Z, Ma Y, Shao C, Wang W, Tang YD (2023) Short sleep duration and the risk of nonalcoholic fatty liver disease/metabolic associated fatty liver disease: a systematic review and meta-analysis. Sleep Breath = Schlaf Atmung 27(5):1985–1996. https://doi.org/10.1007/s11325-022-02767-z
32. Younossi ZM, Golabi P, Paik JM, Henry A, Van Dongen C, Henry L (2023) The global epidemiology of nonalcoholic fatty liver disease (NAFLD) and nonalcoholic steatohepatitis (NASH): a systematic review. Hepatology (Baltimore MD) 77(4):1335–1347. https://doi.org/10.1097/HEP.0000000000000004
33. Zhang SQ, Tian D, Hu CY, Meng YH (2022) Chlorogenic Acid Ameliorates High-Fat and High-Fructose Diet-Induced Cognitive Impairment via Mediating the Microbiota-Gut-Brain Axis. J Agric Food Chem 70(8):2600–2615. https://doi.org/10.1021/acs.jafc.1c07479
34. Zhao Z, Nelson AR, Betsholtz C, Zlokovic BV (2015) Establishment and Dysfunction of the Blood-Brain Barrier. Cell 163(5):1064–1078. https://doi.org/10.1016/j.cell.2015.10.067
35. Zlokovic BV (2008) The blood-brain barrier in health and chronic neurodegenerative disorders. Neuron 57(2):178–201. https://doi.org/10.1016/j.neuron.2008.01.003

Figures

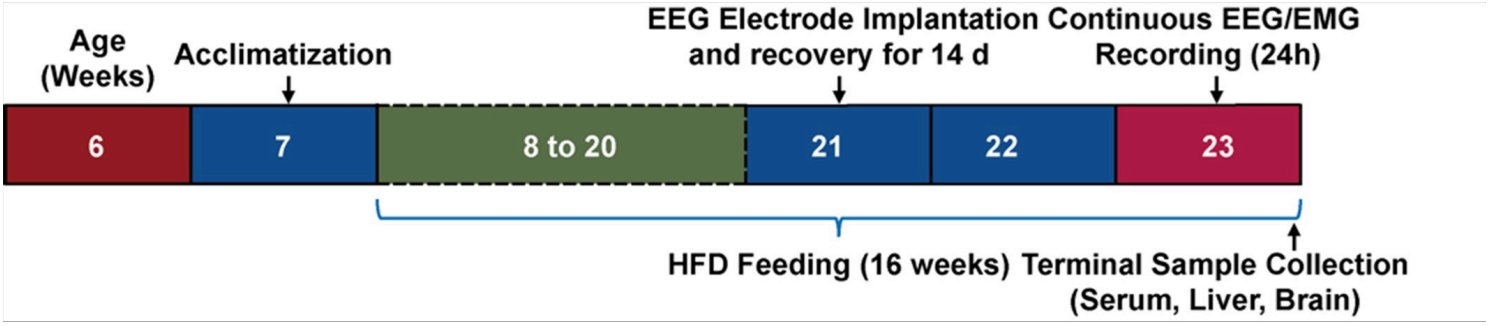


Figure 1

Schematic diagram of the experimental protocol

Mice were maintained on a CD or HFD for 16 weeks (from 8 to 24 weeks of age). At 21 weeks of age, mice underwent EEG/EMG electrode implantation and recovered for 14 days before 24-h continuous video-EEG/EMG recording (at 23 weeks of age). Terminal serum, liver, and brain samples were collected for subsequent analyses. CD, control diet; HFD, high-fat die; EEG, Electroencephalography; EMG: Electromyography.

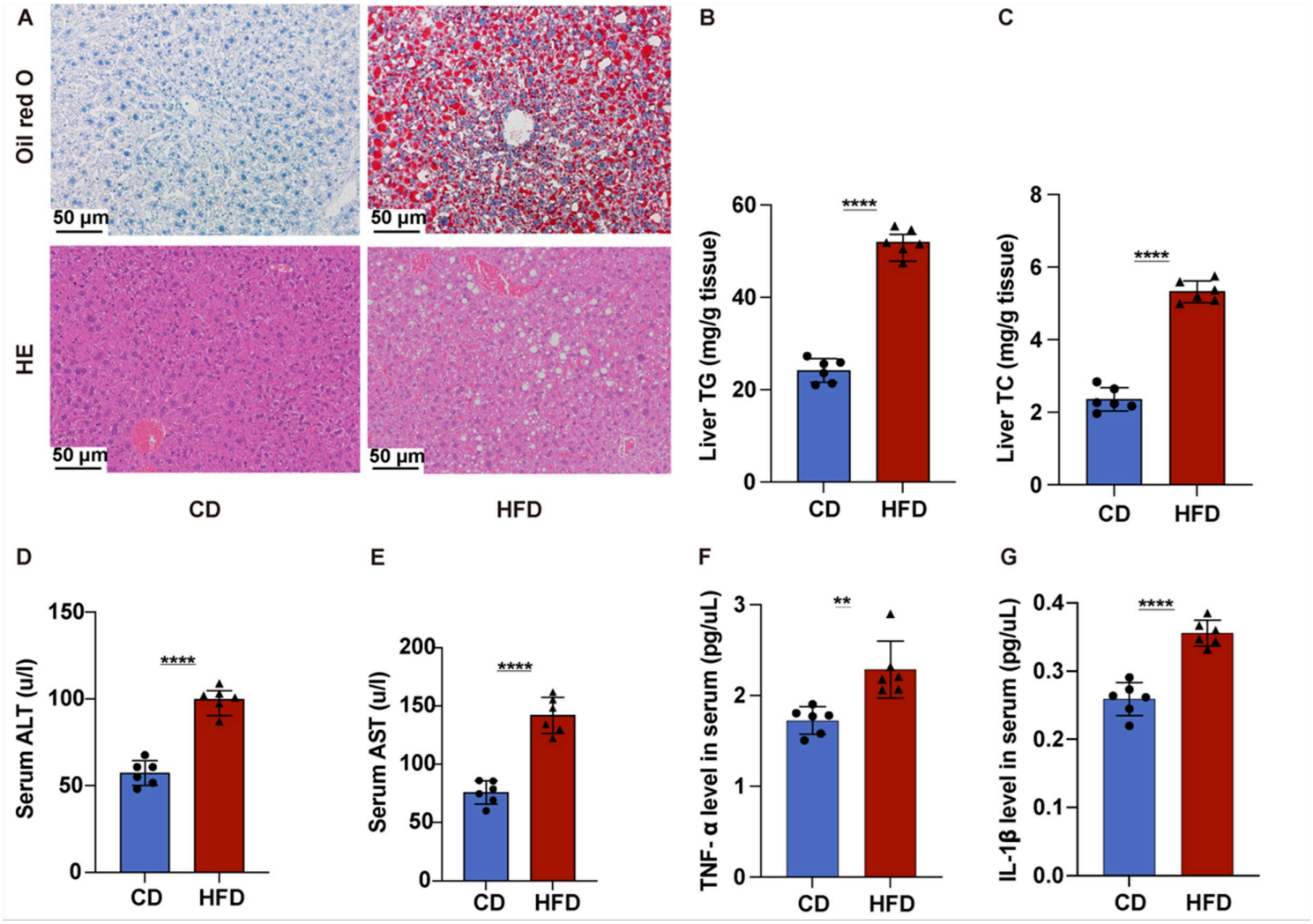


Figure 2

High-fat diet induces hepatic steatosis and metabolic dysregulation

(A) Representative images of ORO staining (top) showing lipid droplets and HE staining (bottom) of liver sections from CD and HFD mice (Scale bar = 50 μm). (B, C) Quantification of hepatic TG (B) and TC (C) levels (*n* = 6 per group). (D, E) Serum levels of liver enzymes ALT (D) and AST (E) (*n* = 6 per group). (F, G) Serum levels of pro-inflammatory cytokines TNF-α (F) and IL-1β (G) (*n* = 6 per group). Data are presented as mean ± SD. Statistical significance was determined by unpaired two-tailed Student's *t*-test: ** $p < 0.01$, **** $p < 0.0001$. CD, control diet; HFD, high-fat diet; ORO, Oil Red O; HE, Hematoxylin and Eosin; TG, triglyceride; TC, total cholesterol; ALT, alanine aminotransferase; AST, aspartate aminotransferase; TNF-α, tumor necrosis factor- alpha; IL-1β, interleukin-1 beta.

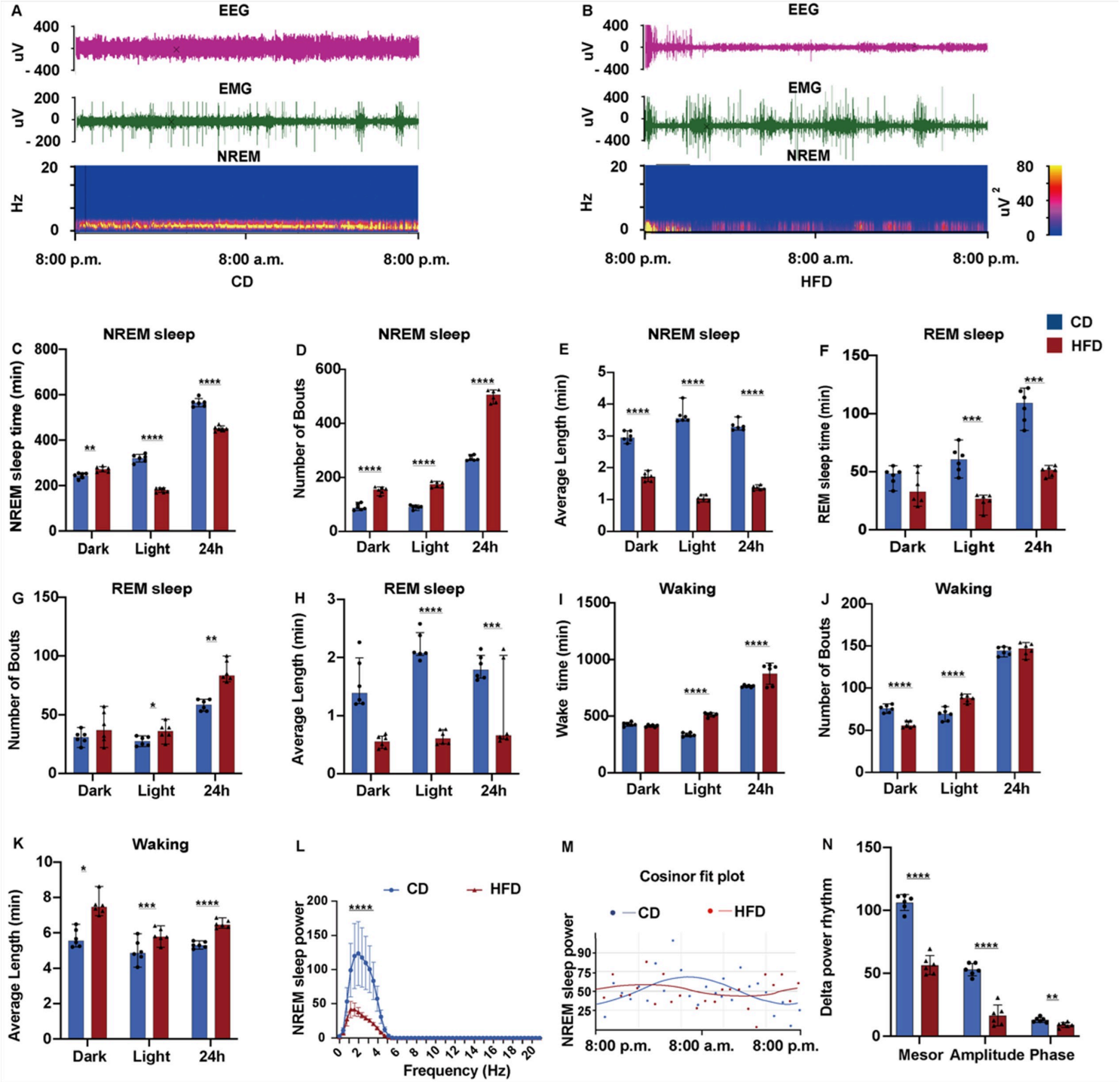


Figure 3

High-fat diet disrupts sleep architecture and circadian rhythmicity

(A, B) Representative 24-h EEG (top) and EMG (middle) traces, with corresponding sleep–wake state hypnograms (bottom) for CD (left) and HFD (right) mice.

(C–E) NREM sleep parameters: (C) total sleep time, (D) number of bouts, and (E) average bout length during dark, light, and 24-h periods.

(F–H) REM sleep parameters: (F) total sleep time, (G) number of bouts, and (H) average bout length during dark, light, and 24-h periods.

(I–K) Wakefulness parameters: (I) total wake time, (J) number of bouts, and (K) average bout length during dark, light, and 24-h periods.
(L) Power spectral density of NREM sleep (frequency on x-axis, power on y-axis) for CD (blue) and HFD (red) mice.
(M-N) Cosinor fit plot and circadian rhythmicity of NREM sleep delta power showing mesor, amplitude, and phase for CD (blue) and HFD (red) mice.
Data are presented as mean ± SD for normally distributed variables and median [interquartile range] for non-normally distributed variables (REM mean duration, Dark and 24h). Normally distributed data were compared using unpaired two-tailed Student's *t*-test; non-normally distributed data were compared using Mann-Whitney *U* test. A two-way repeated-measures ANOVA (frequency × diet) was performed on absolute power values, followed by post-hoc comparisons at 1–4 Hz. $n = 6$ per group. * $p < 0.05$, ** $p < 0.01$, *** $p < 0.001$, **** $p < 0.0001$. CD, control diet; HFD, high-fat diet; NREM, non-rapid eye movement; REM, rapid eye movement.

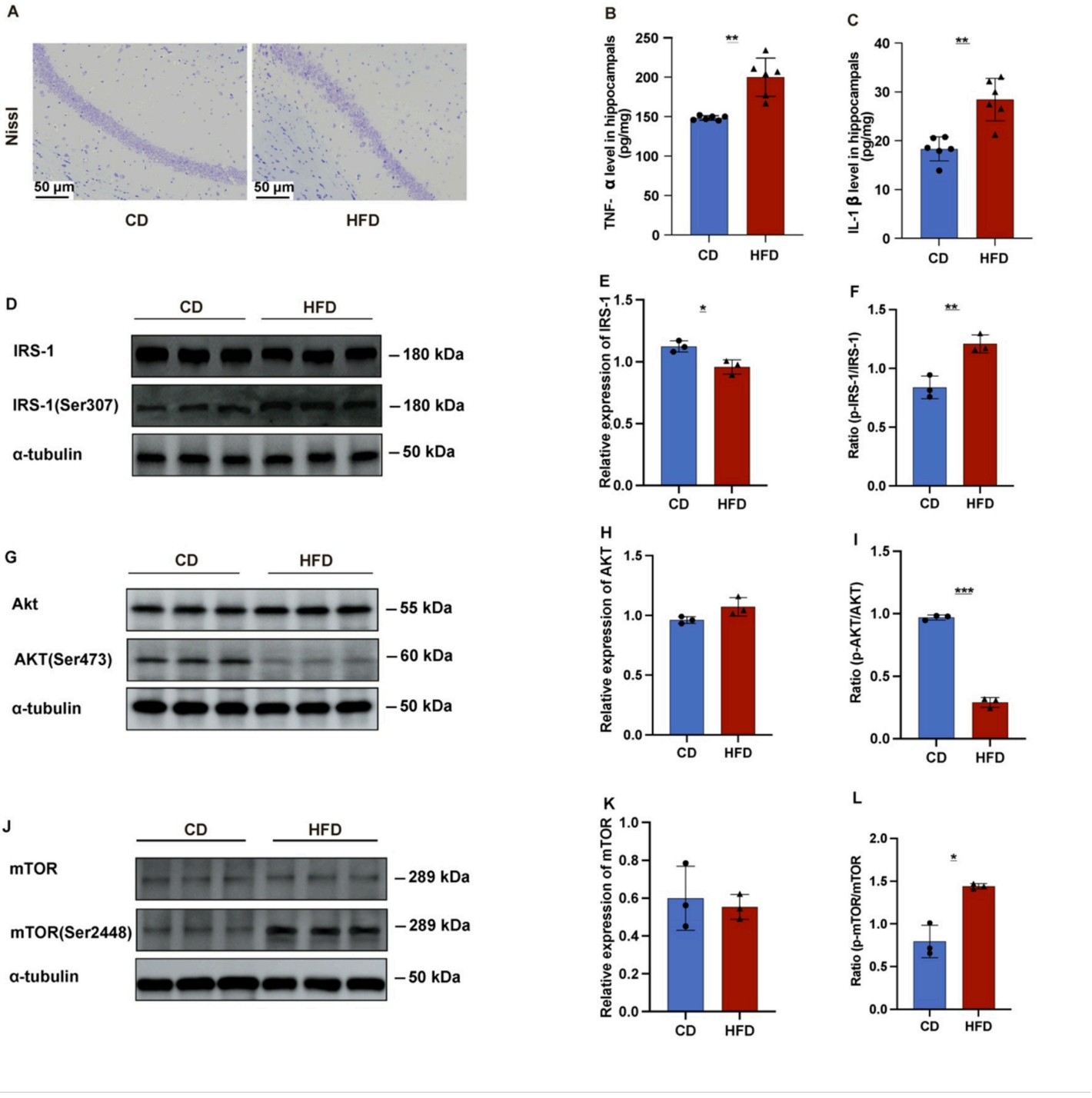


Figure 4

High-fat diet induces neuroinflammation and insulin resistance in the hippocampus
(A) Representative Nissl staining images of the hippocampus from CD and HFD mice (Scale bar = 50 μm). The Nissl staining revealed bluish-purple neuronal Nissl bodies and nuclei against a light blue background. Neurons in the CD group exhibited an orderly arrangement and regular morphology. In contrast, the HFD group showed disorganized neurons with irregular morphology.

(B, C) Quantification of TNF-α (B) and IL-1β (C) levels in hippocampal tissue (*n*= 6 per group).
(D–F) Western blot analysis and quantification of IRS-1 Ser307 phosphorylation and total IRS-1 levels. (D) Representative blots. (E) Relative expression of IRS-1 (normalized to α-tubulin). (F) Ratio of p-IRS-1 to total IRS-1 (*n*= 3 independent biological replicates).
(G–I) Western blot analysis and quantification of Akt Ser473 phosphorylation and total Akt levels. (G) Representative blots. (H) Relative expression of Akt (normalized to α-tubulin). (I) Ratio of p-Akt to total Akt (*n* = 3 independent biological replicates).
(J–L) Western blot analysis and quantification of mTOR Ser2448 phosphorylation and total mTOR levels. (J) Representative blots. (K) Relative expression of mTOR (normalized to α-tubulin). (L) Ratio of p-mTOR to total mTOR (*n* = 3 independent biological replicates).
Data are presented as mean ± SD. Statistical significance was determined by unpaired two-tailed Student's *t*-test: * $p < 0.05$, ** $p < 0.01$, *** $p < 0.001$. CD, control diet; HFD, high-fat diet; TNF-α, tumor necrosis factor- alpha; IL-1β, interleukin-1 beta; p-IRS-1, phosphorylated IRS-1; p-Akt, phosphorylated Akt; p-mTOR, phosphorylated mTOR.

Supplementary Files

This is a list of supplementary files associated with this preprint. Click to download.

- UncroppedgelsforWesternBlots.docx